NASA Contractor Report 4208

Users' Manual for the Langley High Speed Propeller Noise Prediction Program (DFP-ATP)

M. H. Dunn and G. M. Tarkenton
Planning Research Corporation
Hampton, Virginia

Prepared for
Langley Research Center
under Contract NAS1-18000

National Aeronautics
and Space Administration

**Scientific and Technical
Information Division**

1989

TABLE OF CONTENTS

LIST OF SYMBOLS AND ABBREVIATIONS

vector quantities are denoted by arrows over the symbol

ATP	advanced technology propeller
$\tilde{B}^i$	i = 1,2; components of $\vec{b}$ in direction of principal curvatures
$\vec{b}$	$\|\vec{M}_t + l_1\vec{t}_1$, $b = \|\vec{b}\|$
b_n	$\vec{b} \cdot \vec{n}$
c	speed of sound in undisturbed fluid
CRP	counter-rotation propeller
C_P	power or torque coefficient of propeller
C_T	thrust coefficient of propeller
dB	decibels
dS	element of blade surface area
$f(\vec{x}, t) = 0$, $f(\vec{y}, t) = 0$	equation describing blade surface in reference frame fixed to the undisturbed medium
$F(\vec{y}; \vec{x}, t)$	$f(\vec{y}, t\text{-}r/c) = [f(\vec{y}, t)]_{ret}$
H	local mean curvature of blade surface
h_n	$\|M_n + l_1 \cos q$
$k(\vec{x}, t) = 0$, $k(\vec{y}, t) = 0$	equation of surface defined such that f = 0 and k > 0 produces an open piece of the blade surface
$K(\vec{y}; \vec{x}, t)$	$k(\vec{y}, t\text{-}r/c) = [k(\vec{y}, t)]_{ret}$
$\vec{M}$	local Mach vector based on c, $M = \|\vec{M}\|$
M_{an}	$\vec{M} \cdot \vec{n}$

$\dot{\vec{M}}$	time derivative of $\vec{M}$
M_n	$\vec{M} \cdot \vec{n}$
M_r	$\vec{M} \cdot \hat{\vec{r}}$
$\vec{M}_p$	projection of Mach vector on local normal plane to edges of blade surface, $M_p = \lvert\vec{M}_p\rvert$
$\vec{M}_t$	projection of Mach vector on local tangent plane to blade surface, $M_t = \lvert\vec{M}_t\rvert$
$\vec{n}$, n_i	unit normal to blade surface
NB	number of blades
OASPL	overall sound pressure level
p'	acoustic pressure
p	aerodynamic blade surface pressure
$\dot{p}$	time derivative of p
$p_B(\vec{\eta}, \tau)$	blade surface pressure in blade fixed reference frame
PCA	pitch change axis
Q	percentage chord coordinate
$\vec{r}$, r_i	$\vec{x} - \vec{y}$, $r = \lvert\vec{x} - \vec{y}\rvert$
$\hat{\vec{r}}$, $\hat{r}_i$	$\vec{r}/r$
$\hat{r}_v$	$\hat{\vec{r}} \cdot \vec{v}$
$\hat{\vec{r}}_p$	unit vector in the direction of the projection of $\vec{r}$ onto the local normal plane to the surface edges
SRP	single-rotation propeller
t	observer time

$\vec{t}_1$	projection of $\vec{r}$ onto local plane tangent to blade surface
V_F	forward flight velocity
$\vec{x}$	observer coordinate in ground fixed reference frame
$\vec{y}$	source coordinate in ground fixed reference frame

Greek Symbols

$d\gamma$	element of length on edge of open surface
$\delta(f)$	Dirac delta function
$d\Sigma$	element of acoustic planform area
θ	angle between $\vec{n}$ and $\hat{\vec{r}}$
$\vec{\eta}$	coordinate of blade surface point in blade fixed frame
η_2	spanwise coordinate
Λ	$(1 + M_n^2 - 2M_n\cos\theta)^{1/2}$
$\tilde{\Lambda}$	$(\Lambda^2 + \sin^2\theta)^{1/2}$
Λ_0	$[M_p^2\cos^2\theta + (1 - \vec{M}_p \cdot \hat{\vec{r}}_p\sin\psi)^2]^{1/2}$
$\tilde{\mu}^i$	$i = 1,2$; components of $\vec{M}_t$ in direction of principal curvatures
$\vec{\nu}, \nu_i$	inward geodesic normal of open surface defined by $k>0$ and $f=0$
ρ_0	density of undisturbed fluid
σ_b	length parameter on $f=0$ along $\vec{b}$

σ_{11}, σ_{22}	two components of the tensor $(\vec{t}_1 \vec{t}_1 - \vec{M}_t \vec{M}_t + \vec{t}_1 \vec{M}_t + \vec{M}_t \vec{t}_1)/\tilde{\Lambda}^2$
τ	source time
ψ	angle between $\vec{r}$ and edge of f=0
$\vec{\Omega}, \Omega_i$	$\vec{n} \times \vec{\omega}$
κ_1, κ_2	principal curvatures of the surface f=0
$\kappa_M, \kappa_t, \kappa_b$	normal curvatures along $\vec{M}_t$, $\vec{t}_1$, and $\vec{b}$, respectively
λ	$(\cos\theta - M_n)/\tilde{\Lambda}^2$
λ_1	$(\cos\theta + M_n)/\tilde{\Lambda}^2$
$\vec{\omega}$	angular velocity

INTRODUCTION

In the late 1950's and early 1960's the turbofan became the propulsion device of choice for commercial aircraft fleets. The turbofan offered higher speed and a safer, more comfortable flight than its predecessor, the propeller. These conveniences, however, resulted in a substantial increase in fuel consumption. The uncertaintity of fuel supplies and the high cost of fuel in the 1970's revived interest in propeller driven flight. Researchers were confronted with the task of designing fuel efficient propulsion systems that were capable of sustaining high speed and high altitude flight while maintaining acceptable ground and cabin noise levels. One outcome of this research was the development of the advanced technology propeller (ATP) or propfan. This new generation of propellers features highly loaded blades that are thin and swept back (Figure 1). It is estimated that the ATP will provide a 20 to 25% reduction in fuel consumption while maintaining the positive attributes of the turbofan [1]. A further reduction in fuel consumption can be achieved by eliminating the velocity swirl in the propfan wake. Counter-rotation propeller systems (Figure 2) accomplish this function. Researchers estimate that, after acoustical treatment, the propfan can be made 8% more efficient by employing counter-rotation [2].

For the past several years considerable resources have been allocated by government and industry to produce a propfan design which minimizes noise while maintaining performance. The construction and acoustical testing of new propeller designs is an expensive and time

consuming process. Thus, a tractable, physically realistic analytical method for predicting propeller noise would provide the engineer with a cost effective alternative to the above process.

This work is concerned with the problem of predicting the noise generated by advanced technology propellers operating at transonic/supersonic helical tip speeds, in both the single-rotation and counter-rotation mode. The analytical method is based on two theoretical formulations developed by Farassat [3], [4]. One formulation is appropriate for subsonic sources and the other for transonic and supersonic sources. The computer program that implements these formulations, known as the Dunn-Farassat-Padula Advanced Technology Propeller (DFP-ATP) noise prediction program, was developed at the NASA Langley Research Center by the first author and F. Farassat and S. Padula of LaRC. Input to the program consists of blade kinematic and geometric quantities and either steady or periodically unsteady blade surface pressure. Program output consists of propeller thrust and power coefficients, and the periodic acoustic pressure signatures and acoustic spectra for the thickness, loading and combined noise.

THEORETICAL FORMULATIONS

Small perturbations in fluid quantities due to the motion of a body through an otherwise quiescent, ideal fluid are governed by the equations of linearized acoustics. Therefore, in the region exterior to the body the acoustic pressure, $p'(\vec{x}, t)$, is a solution of the homogeneous wave equation subject to the boundary condition that the fluid cannot penetrate the surface of the body.

Using generalized function theory, the restricted domain of the above problem, i.e, the body's exterior, can be extended to include the entirety of space by the process of embedding [5]. Applying this procedure to the equations of acoustics leads to the Ffowcs Williams-Hawkins equation without the quadrupole term [6]:

$$\frac{1}{c^2}\frac{\bar{\partial}^2 p'}{\partial t^2} - \bar{\nabla}^2 p' = \bar{\nabla}_4 \bullet \left[\vec{Q}|\nabla f|\delta(f)\right] \qquad (1)$$

where

$$\vec{Q} = (-p\,\vec{n}, M_n) \quad , \quad \bar{\nabla}_4 = (\bar{\nabla}, \frac{1}{c}\frac{\bar{\partial}}{\partial t})$$

and the bars over the differential operators denote generalized differentiation. The boundary condition and the pressure on the surface of the body appear as source terms in (1). The advantage of the embedding technique is that the Green's function for the wave equation in unbounded space is

known, thus the solution of (1) can be obtained analytically provided the aerodynamic pressure on the surface of the body is known.

A solution of (1), known as Formulation 1A, that is valid over source regions that move subsonically toward the observer, is given by [3]:

$$p'(\vec{x}, t) = p_T'(\vec{x}, t) + p_L'(\vec{x}, t)$$

where

$$p_T'(\vec{x}, t) = c\rho_0 \int_{f=0} \left[\frac{M_n (r\dot{M}_i \hat{r}_i + cM_r - cM^2)}{r^2 (1-M_r)^3} \right]_{ret} dS \qquad (2)$$

and

$$p_L'(\vec{x}, t) = \frac{1}{c} \int_{f=0} \left[\frac{\dot{p}\cos\theta}{r(1-M_r)^2} \right]_{ret} dS - \int_{f=0} \left[\frac{p(\cos\theta - M_n)}{r^2(1-M_r)^2} \right]_{ret} dS +$$

$$\frac{1}{c} \int_{f=0} \left[\frac{p\cos\theta (r\dot{M}_i \hat{r}_i + cM_r - cM^2)}{r^2 (1-M_r)^3} \right]_{ret} dS \; . \qquad (3)$$

The subscript ret indicates that the terms in the integrands are to be evaluated at the emission (or retarded) time and the integrations are per-

formed over the actual body surface. The functions p_T' and p_L' are referred to, respectively, as the thickness and loading noise components of the total pressure. This formulation is invalid for portions of the body that move toward the observer with transonic speed. A nearly equivalent formulation exists for supersonic sources, however, computational difficulties limit its usefulness. Particularly, instabilities in the numerical evaluation of (2) and (3) occur in regions where the Doppler factor, $1-M_r$, is "small", and it is computationally difficult to differentiate between "nearly" transonic and supersonic source regions. To circumvent these problems Farassat developed equations (4) and (5) below [4]:

$$p_T' = \int_{\substack{F=0\\K>0}} \frac{M_n^2 Q_N'}{\Lambda r^2}\, d\Sigma + \int_{\substack{F=0\\K>0}} \frac{M_n^2 Q_F + Q_F' + Q_F''}{\Lambda r}\, d\Sigma - \int_{\substack{F=0\\K=0}} \frac{M_n^2 Q_E + M_n M_{av}}{\Lambda_0 r}\, d\gamma \qquad (4)$$

$$p_L' = \int_{\substack{F=0\\K>0}} \frac{pQ_N'}{\Lambda r^2}\, d\Sigma + \int_{\substack{F=0\\K>0}} \frac{pQ_F}{\Lambda r}\, d\Sigma + \int_{\substack{F=0\\K=0}} \frac{pQ_E}{\Lambda_0 r}\, d\gamma \qquad (5)$$

where

$$Q_N' = \lambda\left[2\lambda_1\left(\cos\theta - M_n\right)+1\right] ,$$

$$Q_F = \frac{1}{c}\left(2\lambda^2 - \frac{1}{\tilde{\Lambda}^2}\right)\dot{M}_n + 2b^2\kappa_b + \kappa_1\sigma_{11} + \kappa_2\sigma_{22} - 2Hh_n +$$

$$\frac{1}{c}\vec{\Omega}\cdot\left[\frac{\vec{M}_t - \vec{t}_1}{\tilde{\Lambda}^2} - 2\lambda\vec{b} + \left(\frac{1}{\tilde{\Lambda}^2} + 2\lambda\lambda_1\right)\hat{\vec{r}}\right] ,$$

$$Q_F' = 2M_n\left[\frac{1}{c}\left(\lambda\dot{M}_n - \vec{\Omega}\cdot\vec{b}\right) + \kappa_1\tilde{\mu}^1\tilde{B}^1 + \kappa_2\tilde{\mu}^2\tilde{B}^2\right] + \frac{\lambda}{c}\dot{p}_B - b\frac{\partial p_B}{\partial\sigma_B}$$

$$Q_F'' = \frac{1}{c}\left(\dot{M}_n - \vec{\Omega}\cdot\vec{M}_t\right) + \kappa_m M_t^2 - 2HM_n^2$$

and

$$Q_E = \lambda M_{av} + \lambda_1\hat{r}_v$$

This solution is referred to as Formulation 3. The surface integrals of equations (4) and (5) are evaluated over the acoustic planform (or Σ-surface), and the line integrals are computed over the boundary of the acoustic planform. The Σ-surface is generated by the intersection of the surface of the moving body and a sphere, centered at the observer position, $\vec{x}$, whose radius collapses at the speed of sound. This formulation is valid in all regions regardless of the value of the radial Mach number. Due to the complex nature of the integrands, however, equations (2) and (3) can be evaluated much more efficiently in the subsonic regime.

per computes the acoustic pressure generated by advanced technology propellers. The contribution to the total noise attributable to subsonic portions of the propeller surface are computed via (2) and (3), while (4) and (5) are evaluated to determine the contribution from the transonic and supersonic regions of the propeller surface.

COMPUTATIONAL STRATEGY

In this section the computational strategies for the noise prediction process are discussed. The methods were designed to make the overall process as accurate as possible while minimizing the computational time and storage requirements.

The calculations that are described here are based on two assumptions. One, the observer position moves parallel to the propeller axis with the same speed as the aircraft, and two, for CRP predictions, both propellers operate at the same RPM, they have the same number of blades, and their pitch change axes are initially aligned (Figure 3). The CRP restrictions are imposed to facilitate the spectral analysis of the CRP acoustic pressure signal. If the user is interested in CRP predictions where these conditions cannot be satisfied, then the signals from the individual propellers can be obtained by making two separate predictions, one for each propeller. The user can then add the two signals in an appropriate fashion and perform the desired Fourier analysis. In some instances the program can be easily modified to accomodate special circumstances.

To begin the computations, user supplied blade geometry and loading data, which are given as functions of span and percentage chord, are modelled by high order, two dimensional, tensor product, least-squares splines. The software employed for this task is a modified version of the computer programs appearing in reference [7]. The blade surface is then separated

into two regions: the subsonic root region and the supersonic tip region. The spanwise location $\eta_2^* = \frac{1}{\omega}\left(c_*^2 - V_F^2\right)^{1/2}$, where $c_* = (1-\varepsilon)c$ with ε a small parameter supplied by the user, serves as the boundary separating the two regions. This separation point avoids the computational difficulties that were discussed in the previous section. Both regions are then subdivided into equally spaced spanwise and chordwise intervals according to user specifications (Figure 4a). For each resultant panel, the following calculations are performed:

STEP (1) A user-specified number of Gauss-Legendre (GL) nodes are distributed over the panel (Figure 4b).

STEP(2) Blade geometric quantities and the steady portion of the blade surface pressure at each GL node are computed and stored.

STEP(3) For each observer time, the emission time(s) and M_r are calculated at each GL node. If $1-M_r < \varepsilon$ on any GL node at any emission time, then STEP(3A) is performed, otherwise STEP(3B) is performed.

STEP(3A) The panel is subdivided further, according to user specifications, by evenly spaced spanwise and chordwise partitions (Figure 4c) and equations (4) and (5) are used to compute the noise for that observer time. The surface integrals are evaluated by the "collapsing sphere" method [8]. The Γ-curves generated by the method are approximated by piecewise linear functions and the integrals are approximated by the mid-point rule. The line integrals appearing in (4) and (5) are calculated by the trapezoid rule.

STEP(3B) Equations (2) and (3) are used to compute the noise in this case.

The integrals are calculated by Gaussian quadrature based on the nodes computed in STEP(1). The software used to calculate the Gaussian quadrature nodes and weights was taken from [9].

STEP(4) For each observer time, the noise contribution from each panel is summed to form a single blade pressure signature. This is done for the thickness, loading and total noise components. For CRP predictions the above 4 steps are performed twice, once for each propeller. The single blade signatures of the two propellers are then summed according to the superposition principle.

STEP(5) The single blade signatures are shifted and summed to obtain an NB blade periodic acoustic pressure signal, again according to the superposition principle.

STEP(6) The Fourier series of the NB blade signal is computed via Simpson's rule.

STEP(7) Sound pressure levels are computed and written to output as are the NB blade thickness, loading and combined acoustic pressures.

The above steps are depicted schematically in Figure 5. As was mentioned earlier, the integrands of equations (2) and (3) must be evaluated at the emission time. Also, construction of the Σ-surface of equations (4) and (5) is based on a knowledge of the emission times. Thus, it is important to be able to calculate the emission times efficiently. The algorithm employed for this purpose is responsible for approximately one-half of the program's total computational time and is briefly described in appendix A.

PROGRAM DESCRIPTION

In this section the user input specifications, program output and details of the program usage are described.

Operating Instructions

The user input file is associated with the FORTRAN logical unit number 5. All input parameters reside on this file. User input consists of three groups of NAMELIST variables and blade coordinates and loading data. The structure and contents of the input file will be discussed in the ensuing subsections. The standard program output file is associated with the FORTRAN logical unit number 6. Additional output files containing intermediate results are associated with FORTRAN logical unit numbers 7 and 8. The user must open these files in the calling program.

To access the noise prediction program, the user's calling program must have the FORTRAN statement

CALL DFPATP(X , NXDIM)

where X is a one-dimensional dynamic storage array whose dimension, NXDIM, must be at least

$$\max\{\ 3*NOBS + 6*NT + 26*N1S*N2S + 3*\max(N1S,N2S) + 7*(IGAUSS)^2\ ,$$
$$6*NEPTS*(NQPTS+1) + 2*NQPTS\ \}\ .$$

The standard program output consists of a banner page, a one line identifier, NAMELIST parameters, computational grid information, power (or torque) and thrust coefficients, and thickness, loading and combined sound pressure levels and periodic acoustic pressure signatures. In addition, unit 7 contains the single blade pressure signal for SRP predictions. For CRP predictions, unit 7 contains the single blade signal for the forward propeller and unit 8 contains the single blade signal for the aft propeller.

NAMELIST PHYSCAL Parameters

The variables appearing in this NAMELIST describe the physical characteristics of the undisturbed medium and the kinematic properties of the propeller.

Variable	Description
BTIP	Real. Distance from propeller hub to propeller tip in meters.
BINNER	Real. Distance from propeller hub to propeller root in meters.
VF	Real. Propeller forward flight velocity in meters per second.
RPM	Real. Propeller angular velocity in revolutions per minute.
C0	Real. Speed of sound of undisturbed fluid in meters per second.

RHO0	Real. Density of undisturbed fluid in kilograms per cubic meter.
NB	Integer. Number of blades.
NOBS	Integer. Number of observers.
STEADY	Logical. STEADY = .TRUE. ⇒ steady loading. STEADY = .FALSE. ⇒ unsteady loading.
NCRP	Integer. NCRP = 0 ⇒ SRP prediction. NCRP = 1 ⇒ front propeller of CRP prediction. NCRP = 2 ⇒ aft propeller of CRP prediction.
PROPDIS	Real. Distance between CRP propellers in meters (Figure 3).

NAMELIST GRID Parameters

These parameters determine the computational grid for the acoustic calculations.

Variable	Description
NT	Integer. Number of observer time points for single blade pressure signature. NT ≥ 2. Default value: 125*NB.
NS	Integer. Number of spectral levels to be output. Default value: 30.

N1SUB	Integer. Number of equally spaced spanwise intervals for the subsonic portion of the blade (Figure 4a). Default value: 2.
N1SUP	Integer. Number of equally spaced spanwise intervals for the supersonic portion of the blade (Figure 4a). Default value: 2.
N2SUB	Integer. Number of equally spaced percentage chord intervals for the subsonic portion of the blade (Figure 4a). Default value: 4.
N2SUP	Integer. Number of equally spaced percentage chord intervals for the supersonic portion of the blade (Figure 4a). Default value: 4.
N1S	Integer. Number of equally spaced spanwise points for Formulation 3 panels (Figure 4c). Default value: 10.
N2S	Integer. Number of equally spaced percentage chord points for Formulation 3 panels (Figure 4c). Default value: 10.
EPSILON	Real. If EPSILON > $1-M_r$ for some point on a panel then Formulation 3 is used. Default value: 0.05.
IGAUSS	Integer. Order of Gaussian quadrature for computing Formulation 1A integrals (Figure 4b). Default value: 7.

NAMELIST OBSERV Parameters

This NAMELIST contains the observer(s) coordinates.

OBS(I, J) Real. I-th cartesian coordinate, in meters, of the J-th observer with respect to the aircraft-fixed reference frame (see below). I = 1,2,3 and J = 1,...,NOBS.

Blade Loading and Geometry Input Specifications

Details of the blade geometry input begin with a discussion of the coordinate systems used in the acoustic calculations. They are the ground fixed $\vec{x}$-frame, the aircraft fixed $\vec{X}$-frame and the blade fixed $\vec{\eta}$-frame (Figure 12). Initially, the propeller hub center is at the origin of the $\vec{x}$-frame. The x_3 axis and the propeller axis coincide, with positive x_3 in the direction of flight. The propeller disk lies in the x_1-x_2 plane initially and x_1 and x_2 are defined such that the $\vec{x}$-frame is right-handed. The positive sense of rotation is defined to be from the x_1-axis to the x_2-axis. The $\vec{X}$-frame is identical to the $\vec{x}$-frame initially and moves in the forward flight direction with speed V_F. The observer coordinates are given in the $\vec{X}$-frame. The origin of the blade fixed $\vec{\eta}$-frame coincides with the origin of the $\vec{X}$-frame at all times. The η_3-axis lies along the propeller axis, the η_2-axis lies along the pitch change axis, and η_1 is chosen so that the $\vec{\eta}$-frame is right-handed.

The blade geometry input is specified with respect to the blade fixed frame. Airfoil sections are generated by cutting the PCA with planes perpendicular to the PCA. For each section the twist, α, in degrees, the local chord length, CHORD, in meters, and the η_1 and η_3 coordinates of the lead-

ing edge, η_1-LE and η_3-LE, in meters, are specified (Figure 13a and 13b). The cutting planes are given by η_2= constant (meters). The first cutting plane is η_2 = BINNER and the last is η_2 = BTIP. The coordinates of the airfoil section are nondimensionalized by the local chord length. The upper and lower coordinates of the airfoil, $y_U(Q)$ and $y_L(Q)$, are given as functions of percentage chord, Q, with Q = 0 corresponding to the leading edge and Q = 1 corresponding to the trailing edge (Figure 13c).

Blade surface pressure can be either steady or periodically unsteady. The user must supply the steady portion of the surface pressure at each (η_2, Q) point that is input. For each spanwise cut the upper and lower steady surface pressure, $p_U(Q)$ and $p_L(Q)$, are input as functions of percentage chord. These quantities are nondimensionalized by $\rho_0\omega^2 BTIP^2$. If the surface pressure is unsteady, then it must be of the form $p(\eta_2, Q)[1 + g(t)]$. The function g is assumed to be periodic with period 2π. The user specifies g in tabular form, $(t_i, g(t_i))$, with the first time point equal to 0 (zero) and the last equal to 2π.

The geometry and loading portion of the input file has the following format:

(1) Number of η_2 = constant cutting planes (NEPTS), number of Q points per airfoil section (NQPTS), number of time points for unsteady loading (NTPTS). -- FORMAT(1X,3I10) --
The chordwise Q points should be biased toward the leading edge and the spanwise η_2 points should be biased toward the tip.

(2) Percentage chord grid. -- FORMAT(1X,E15.7)

$Q_1 = 0.0$

•

•

•

$Q_{NQPTS} = 1.0$

(3) η_2, CHORD, α, η_1-LE, η_3-LE -- FORMAT(1X,5E15.7)

$y_L(Q_1)$, $y_U(Q_1)$, $p_L(Q_1)$, $p_U(Q_1)$ -- FORMAT(1X,4E15.7)

•

•

•

$y_L(Q_{NQPTS})$, $y_U(Q_{NQPTS})$, $p_L(Q_{NQPTS})$, $p_U(Q_{NQPTS})$

(4) Item (3) is repeated for each of the NEPTS spanwise points.

(5) If the surface pressure is unsteady, then g(t) is input here.

t_1, $g(t_1)$ -- FORMAT(1X,2E15.7)

•

•

•

t_{NTPTS}, $g(t_{NTPTS})$

(6) If the noise prediction is for a CRP configuration, then items (1) to (5) are repeated for the aft propeller. The location of the aft propeller data within the input file is described in the Input File Structure subsection.

The geometric and loading input parameters are summarized below.

Variable	Description
NEPTS	Integer. Number of spanwise data points. Recommend: 20-30.
NQPTS	Integer. Number of percentage chord data points Recommend: 30-50.
NTPTS	Integer. Number of time points for unsteady loading data. Recommend: 20-50.
Q	Real. Percentage chord data points. Nondimensionalized by CHORD. $0 \leq Q \leq 1$.
η_2	Real. Spanwise data points in meters. BINNER $\leq \eta_2 \leq$ BTIP.
CHORD	Real. Local chord length in meters.
α	Real. Local twist angle in degrees.
η_1 - LE	Real. η_1 coordinate of leading edge in meters.
η_3 - LE	Real. η_3 coordinate of leading edge in meters.
$y_L(Q)$	Real. Coordinate of lower airfoil surface. Nondimensionalized by CHORD.

$y_U(Q)$	Real. Coordinate of upper airfoil surface. Nondimensionalized by CHORD.
$p_L(Q)$	Real. Steady pressure component on lower airfoil surface. Nondimensionalized by $\rho_0 BTIP^2 \omega^2$.
$p_U(Q)$	Real. Steady pressure component on upper airfoil surface. Nondimensionalized by $\rho_0 BTIP^2 \omega^2$.
t	Real. Time coordinate for unsteady portion of blade pressure. Nondimensionalized by $2\pi/\omega$. $0 \leq t \leq 2\pi$.
g(t)	Real. Unsteady portion of blade pressure. Nondimensional.

Input File Structure

The structure of the user input file is described here. Two sample input files are presented in the next section.

(A) SRP predictions

(1) An 80 character identifier with A80 format
(2) NAMELIST PHYSCAL -- Note that NCRP must be equal to 0.
(3) NAMELIST GRID
(4) Blade coordinates and steady portion of the blade loading data
(4') If STEADY = .FALSE., then the unsteady portion of the blade loading data appears here.
(5) NAMELIST OBSERV

(B) CRP predictions

(1) An 80 character identifier with A80 format

(2) PHYSCAL for forward propeller. -- NCRP must be equal to 1.

(3) GRID for forward propeller

(4) Forward propeller blade coordinates and steady portion of the blade loading data

(4') If STEADY = .FALSE., then the unsteady portion of the forward propeller blade loading data appears here.

(5) OBSERV -- The observer(s) coordinates are based on the hub of the forward propeller being at the origin of the aircraft fixed frame (Figure 3).

(6) PHYSCAL for aft propeller -- NB and NOBS must be the same for both propellers, NCRP must be equal to 2, and RPM for the aft propeller must be the negative of the forward propeller RPM.

(7) GRID for aft propeller -- NT must be the same for both propellers.

(8) Aft propeller blade coordinates and steady portion of the blade loading data

(8') If STEADY = .FALSE., then the unsteady portion of the aft propeller blade loading data appears here.

(9) OBSERV -- These data should be identical to the data for the forward propeller.

EXAMPLES

(A) *SRP prediction*

To illustrate the SRP prediction capability, the noise generated by a model SR3 propeller was computed. The steady loading used in the calculations was obtained from Denton's code [10]. The computed power and thrust coefficients were $C_P = 1.068$ and $C_T = 0.250$. The overall sound pressure level was OASPL = 142.15 dB. Graphs of the sound pressure level harmonics and periodic acoustic pressure signals for the thickness, loading and total noise components can be seen in Figures 6, 7, and 8. The input stream for this example is shown below.

```
SRP PREDICTION--SR3 PROPELLER
$PHYSCAL
BTIP = 0.312,
BINNER = 0.0936,
VF = 241.2,
RPM = 7878.4,
C0 = 310.5,
RHO0 = 0.457,
NB = 4,
NOBS = 1,
STEADY = .TRUE.,
NCRP = 0,
PROPDIS = 0.0,
$END
$GRID
NT = 500,
```

```
NS = 30,
N1SUB = 2,
N1SUP = 3,
N2SUB = 4,
N2SUP = 4,
N1S = 10,
N2S = 10,
EPSILON = 0.05,
IGAUSS = 7,
$END
•-------blade  geometry
•---------and  loading
•-------------data
$OBSERV
OBS(1,1) = 0.810,
OBS(2,1) = 0.0,
OBS(3,1) = -0.20,
$END
```

(B) *CRP prediction*

These results were generated by a model advanced counter rotation propeller system. The blade loading, which includes the aerodynamic interaction between the forward and aft propeller, was obtained from Adamczyk's Euler code [11]. For the forward propeller C_P = 1.225 and C_T = 0.332, and for the aft propeller C_P = 1.296 and C_T = 0.375. The OASPL was 146.33 dB. Graphs of the noise components appear in Figures 9, 10, and 11. The input file is presented below.

```
CRP PREDICTION
$PHYSCAL
BTIP = 0.3064,
BINNER = 0.137,
VF = 242.9,
RPM = 8283,
C0 = 338.3,
RHO0 = 1.039,
NB = 8,
NOBS = 1,
STEADY = .TRUE.,
NCRP = 1,
PROPDIS = 0.1037,
$END
$GRID
NT = 1000,
NS = 30,
N1SUB = 2,
N1SUP = 2,
N2SUB = 4,
N2SUP = 4,
N1S = 10,
N2S = 10,
EPSILON = 0.05,
IGAUSS = 7,
$END
•-----forward  blade
•-----geometry  and
•------loading  data
$OBSERV
OBS(1,1) = 0.800,
OBS(2,1) = 0.0,
OBS(3,1) = -0.05,
$END
----- continued on next column
```

```
$PHYSCAL
BTIP = 0.2937,
BINNER = 0.1322,
VF = 242.9,
RPM = -8283,
C0 = 338.3,
RHO0 = 1.039,
NB = 8,
NOBS = 1,
STEADY = .TRUE.,
NCRP = 2,
PROPDIS = 0.1037,
$END
$GRID
NT = 1000,
NS = 30,
N1SUB = 2,
N1SUP = 2,
N2SUB = 4,
N2SUP = 4,
N1S = 10,
N2S = 10,
EPSILON = 0.05,
IGAUSS = 7,
$END
•--------aft  blade
•------geometry  and
•-------loading  data
$OBSERV
OBS(1,1) = 0.800,
OBS(2,1) = 0.0,
OBS(3,1) = -0.05,
$END
```

DISCUSSION

The effects of varying the computational grid parameters N1SUB, N1SUP, N2SUB, N2SUP, IGAUSS, N1S, N2S and EPSILON have been studied and the results reported in reference [12]. Though the study was not exhaustive, it was determined that acceptable accuracy levels could be attained without the consumption of large amounts of computer resources by using the default values listed in the Program Description section. Furthermore, the authors speculate that a comprehensive grid study will not improve the efficiency of the program to an appreciable degree. To some extent, the choice of these parameters is problem dependent. For example, in situations for which the "sonic line", η_2^*, is closer to the root of the propeller than the tip, the user would be justified in adding one more spanwise interval to the supersonic region of the blade, i.e., set N1SUP equal to 3, and for strictly subsonic predictions adequate results may be obtained by reducing IGAUSS, which would result in a substantial decrease in computational time. However, for most propfans operating at their cruise conditions, the default parameters will yield satisfactory noise predictions.

Comparisons between the theoretical formulations described here and experimental data, both wind tunnel and actual flight data, have been conducted [12]. Measured acoustic data, however, usually contain the effects of nearby hard surface reflection, wave propagation in the fuselage boundary layer or other physical phenomena as well as additional sources of noise such as engines. To adequately model the noise produced in situa-

tions where these effects are important, the noise prediction program should be used in conjunction with other analytical or empirical techniques that sufficiently describe the above physical aspects.

In summary, an efficient computational method for predicting the noise produced by high speed, advanced technology propellers is presented. This new generation of propellers features thin and highly swept blades. Therefore, the noise generated by the propfan can be adequately modelled by linear acoustics. Two analytical solutions of the equations of linear acoustics have been developed by Farassat. One solution, Formulation 3, describes the noise produced by transonic and supersonic propeller motion and the other, Formulation 1A, describes the noise generated by subsonic propeller motion. The program decides automatically which of the two solutions to calculate. The calculations were designed to make the evaluation of the integrals appearing in equations (2) to (5) as accurate as possible while minimizing CPU resources and computer memory requirements. In addition, efforts were made to keep user interaction simple and program output descriptive.

APPENDIX A Emission Time Calculation

For a given observer time, t, consider a particular source point and observer point pair. If sound is emitted from the source at time τ and arrives at the observer at time t then τ is called the emission time (or retarded time). Let $\vec{y}(\tau)$ and $\vec{x}(t)$ be the cartesian coordinates of the source point and the observer point, respectively, then, since the motion of the source and observer are known, the emission time can be determined from the equation

$$c(t - \tau) = | \vec{x}(t) - \vec{y}(\tau) | . \qquad (6)$$

For propeller motion, equation (6) can be written as

$$A\phi^2 + B\phi + C + \cos(\phi + D) = 0 , \qquad (7)$$

where $\phi = \omega(\tau - t)$ and the coefficients A, B, C, and D are known functions of the source and observer positions and the parameters of motion. Equation (6) or (7) is referred to as the "retarded time equation". Note that for propeller motion the emission time appears as an implicit variable in the retarded time equation. Equation (7) cannot be inverted analytically, therefore the emission times must be determined through a numerical technique.

It was previously mentioned that for every observer time comprising the acoustic pressure period, the emission time(s) must be calculated for each source point on the propeller blade computational grid. For typical

noise predictions, the retarded time equation must be solved on the order of 10^6 to 10^7 times accounting for nearly 50 percent of the program's total computational time. The algorithm outlined below was designed to exhaustively search for the solutions of the retarded time equation in an efficient manner.

Let $h(\phi) = A\phi^2 + B\phi + C + \cos(\phi + D)$. Then, solutions of $h(\phi) = 0$ are sought such that $\frac{\phi}{\omega} < 0$. Due to causality, only solutions of this type are physically plausible. The solutions of $h = 0$ are found by a hybrid Bisection/Newton method. Since multiple solutions are possible, it is necessary to obtain "close" initial estimates for each root so that Newton's method can effectively locate all of the solutions. This is accomplished by finding intervals in which the curvature of h does not change sign. Within such intervals, h exhibits parabolic behavior. The function is then sampled at the endpoints of an interval, and several tests are conducted to determine if there are zero, one or two roots in the interval. If roots are detected in the interval, then h is approximated by a parabola and the root(s) of the parabola is (are) used as the initial estimate(s) for Newton's method. Newton's method can be unstable if $\frac{dh}{d\phi}$ is "small" in some neighborhood of the root, thus an alternative method is required for these situations. The Bisection method is used to further refine the estimate before using Newton's method when $\frac{dh}{d\phi}$ is "small". This procedure is repeated for each interval in which the curvature does not change sign.

REFERENCES

[1] W. E. Arndt January 1984 *Aerospace America*, 100 - 103. Propfans Go Full Scale.

[2] E. Bradley et al. 1982 *NASA Technical Memorandum* 82983. Technology and Benefits of Aircraft Counter Rotation Propellers.

[3] F. Farassat and G. P. Succi 1983 *Vertica* 7, 309 - 320. The Prediction of Helicopter Rotor Discrete Frequency Noise.

[4] F. Farassat 1985 *AGARD-CP*-366 (10), 1 - 15. Theoretical Analysis of Linearized Acoustics and Aerodynamics of Advanced Supersonic Propellers.

[5] F. Farassat 1977 *Journal of Sound and Vibration* 55, 165 - 193. Discontinuities in Aerodynamics and Aeroacoustics: The Concept and Applications of Generalized Derivatives.

[6] J. E. Ffowcs Williams 1984 *IMA Journal of Applied Mathematics* 32, 113 - 124. The Acoustic Analogy - Thirty Years On.

[7] C. de Boor 1978 *A Practical Guide to Splines*. New York: Springer - Verlag.

[8] F. Farassat 1975 *NASA Technical Report* R-451. Theory of Noise Generation From Moving Bodies with an Application to Helicopter Rotors.

[9] S. Conte and C. de Boor 1965 *Elementary Numerical Analysis: An Algorithmic Approach*. New York: McGraw Hill.

[10] J. Denton and U. Singh 1979 *Von Karman Institute for Fluid Dynamics. VKI Lecture Series 1979-7*. Time Marching Methods for

Turbomachinery Flow Calculation, in Application of Numerical Methods to Flow Calculations in Turbomachines.

[11] M. Celestina, R. Mulac, and J. Adamczyk 1986 *NASA Technical Memorandum* 87200. A Numerical Simulation of the Inviscid Flow Through a Counter-Rotating Propeller.

[12] F. Farassat, M. Dunn, and S. Padula 1987 *Journal of Sound and Vibration* 119, 53 - 79. Advanced Turboprop Noise Prediction Based on Recent Theoretical Results.

[13] W. Zorumski and D. Weir 1986 *NASA Technical Memorandum* 83199 Part 3, Aircraft Noise Prediction Program Theoretical Manual - Propeller Aerodynamics and Noise.

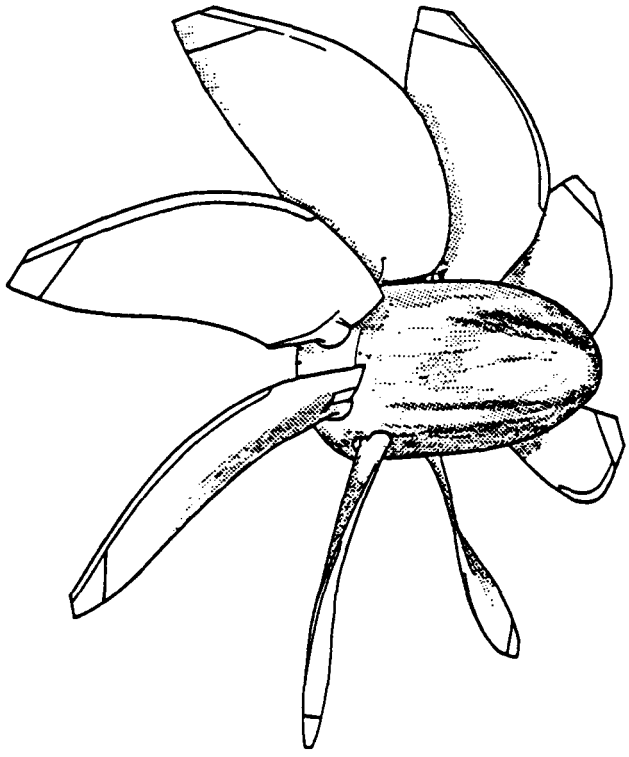

Figure 1: Single Rotation Propeller

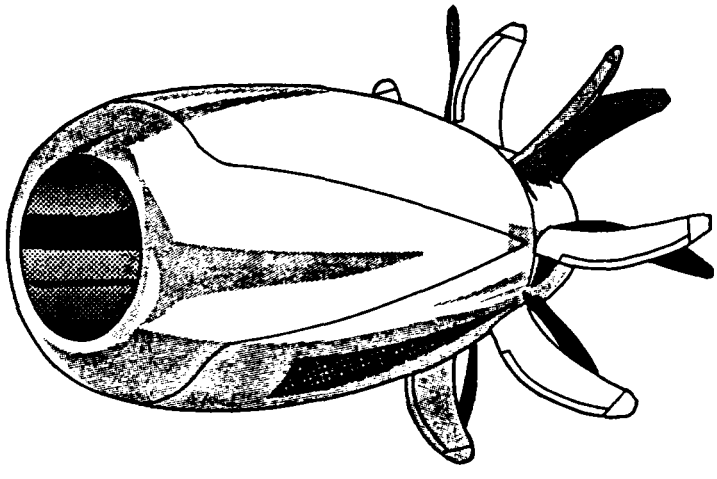

Figure 2: Counter Rotation Propeller System

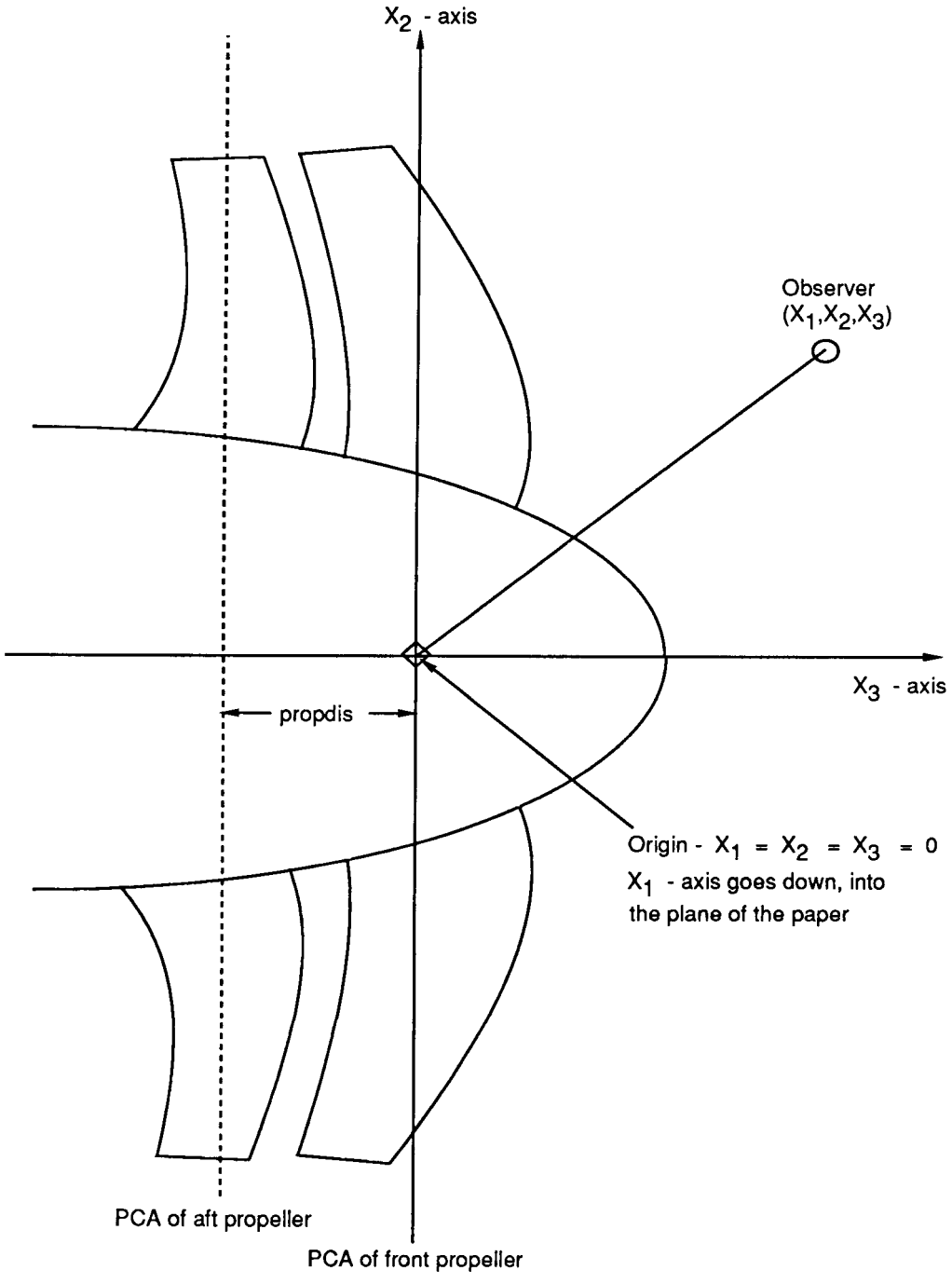

Figure 3: Counter Rotation Configuration - Aircraft Fixed Frame

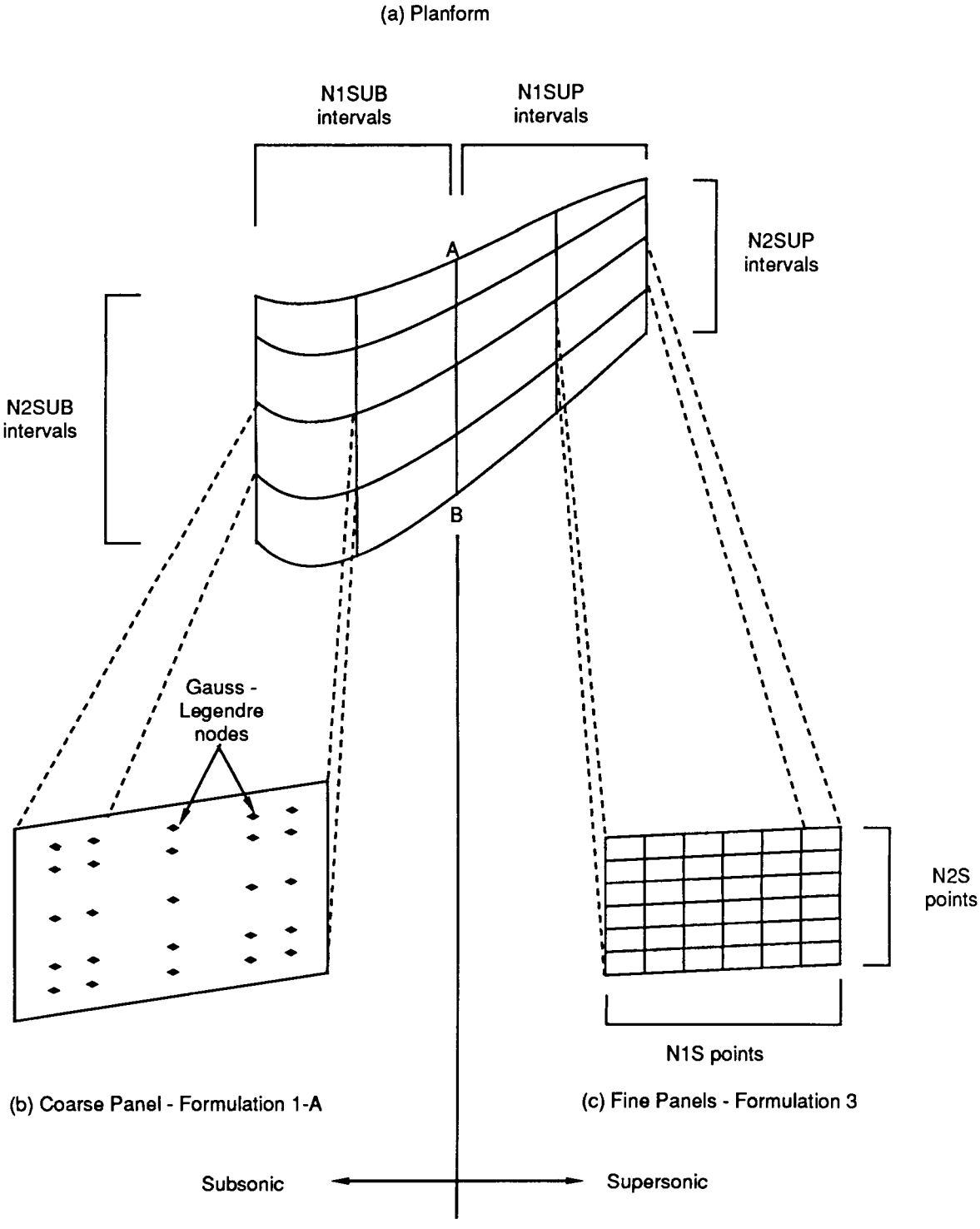

Figure 4: DFP-ATP Computational Grid

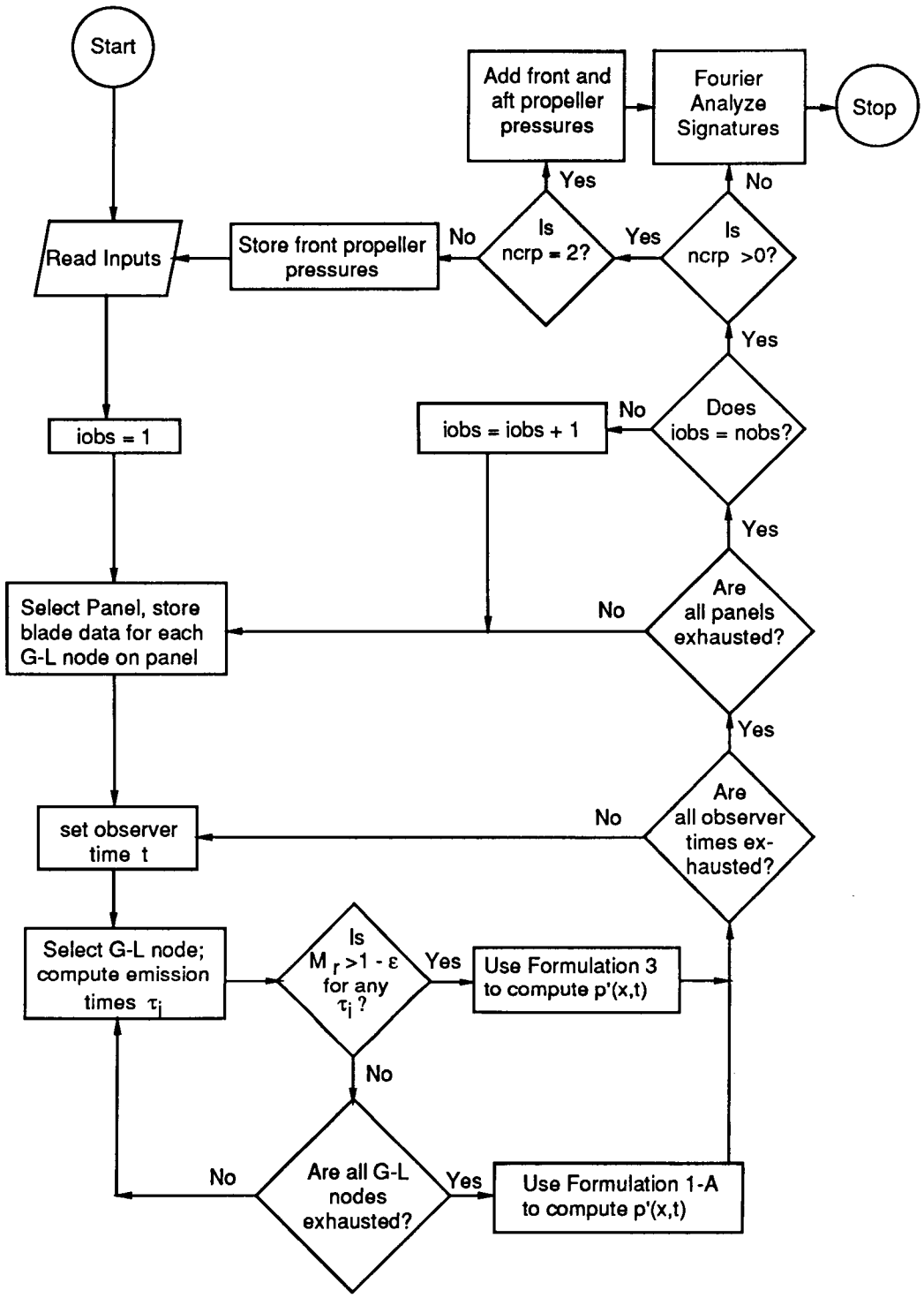

Figure 5: DFP-ATP Flow Chart

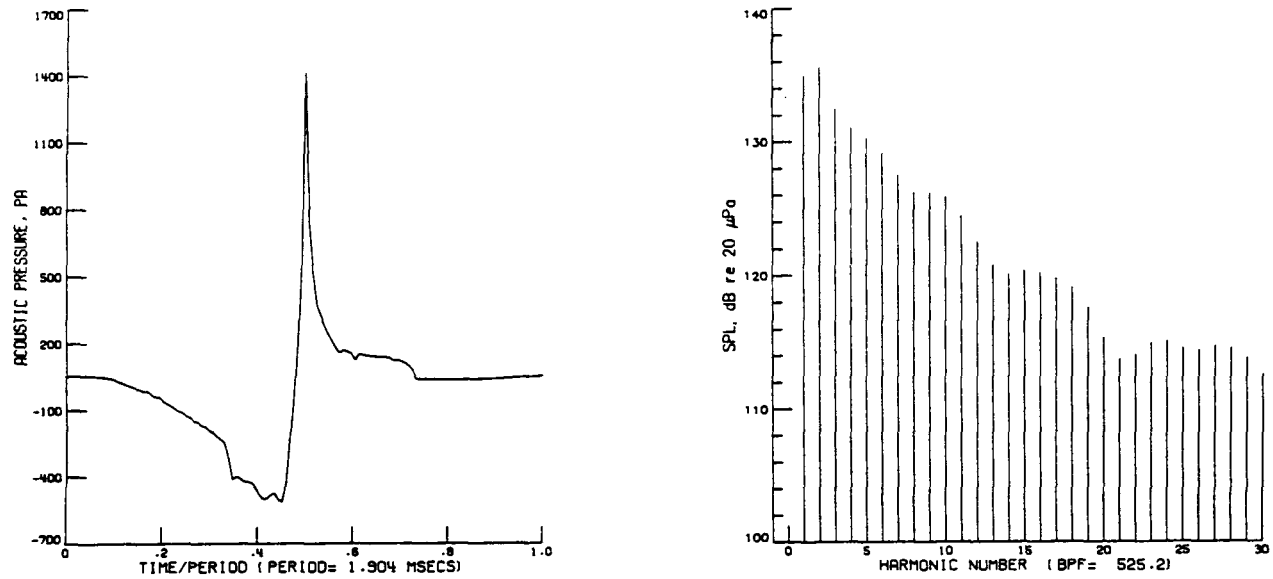

Figure 6: Thickness Noise for Example 1 - Model SR3 Propeller

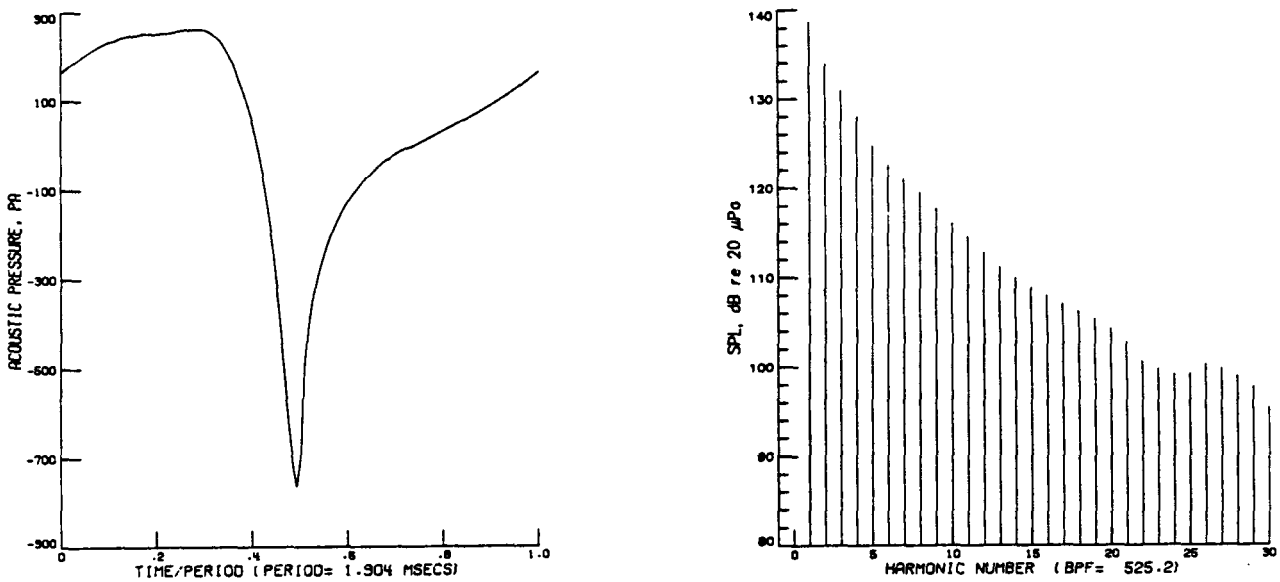

Figure 7: Loading Noise for Example 1 - Model SR3 Propeller

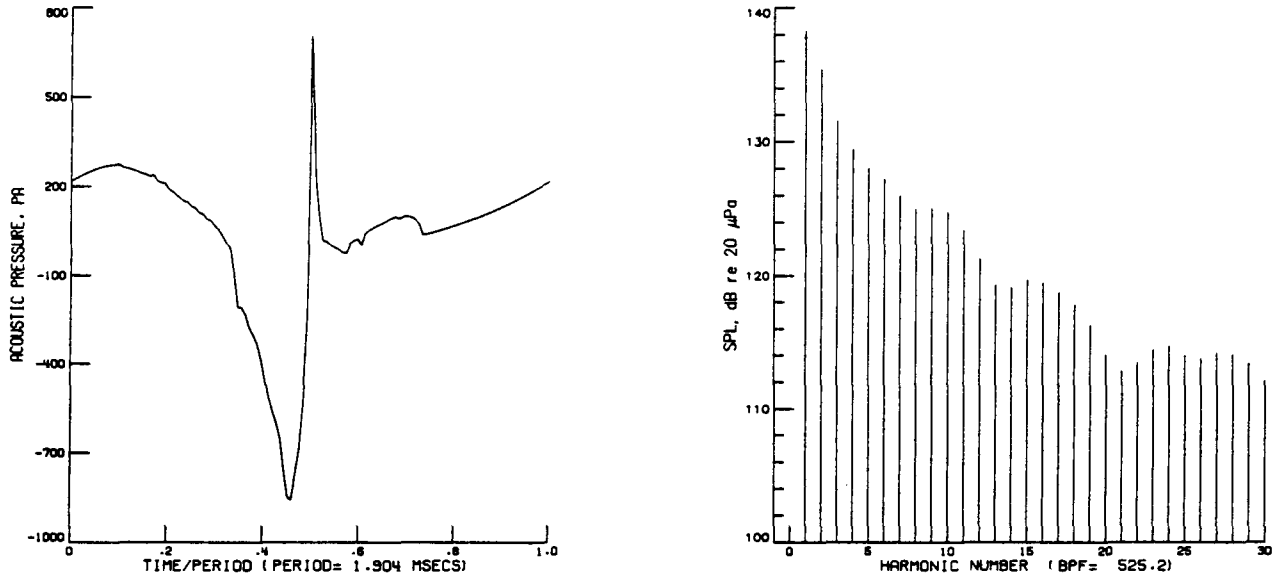

Figure 8: Total Noise for Example 1 - Model SR3 Propeller

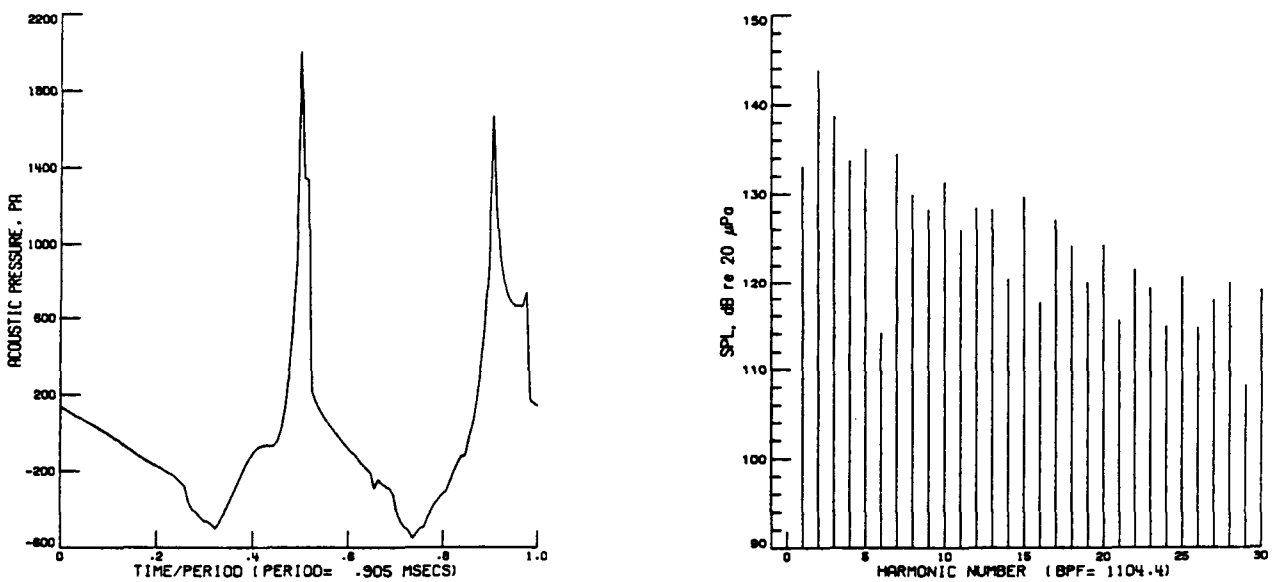

Figure 9: Thickness Noise for Example 2 - Model Counter Rotation Propeller System

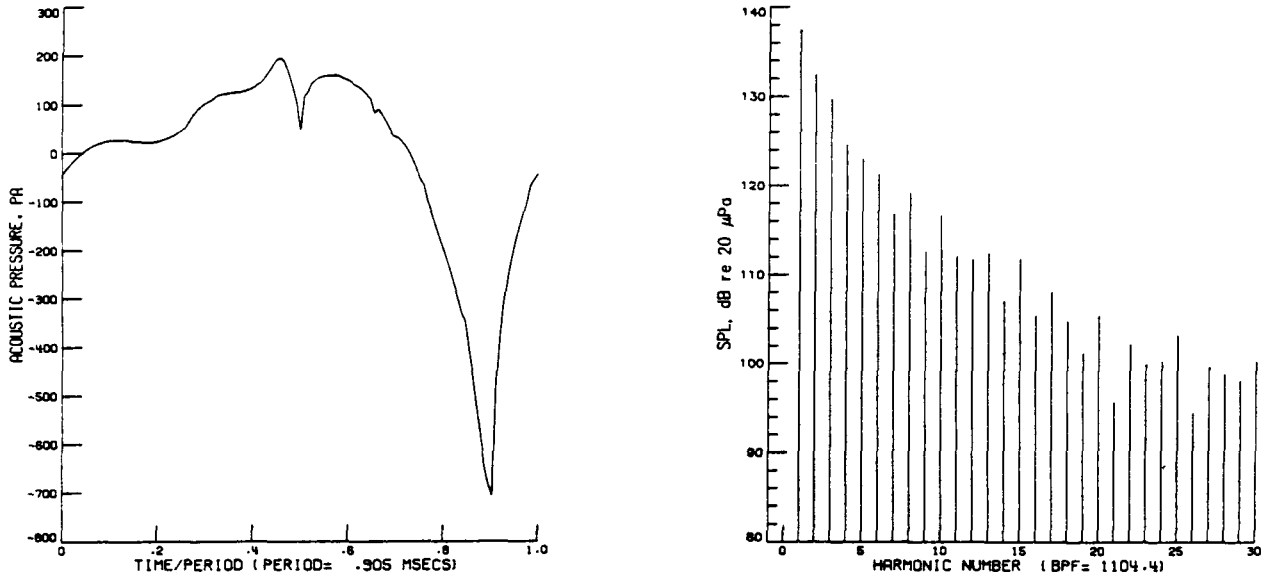

Figure 10: Loading Noise for Example 2 - Model Counter Rotation Propeller System

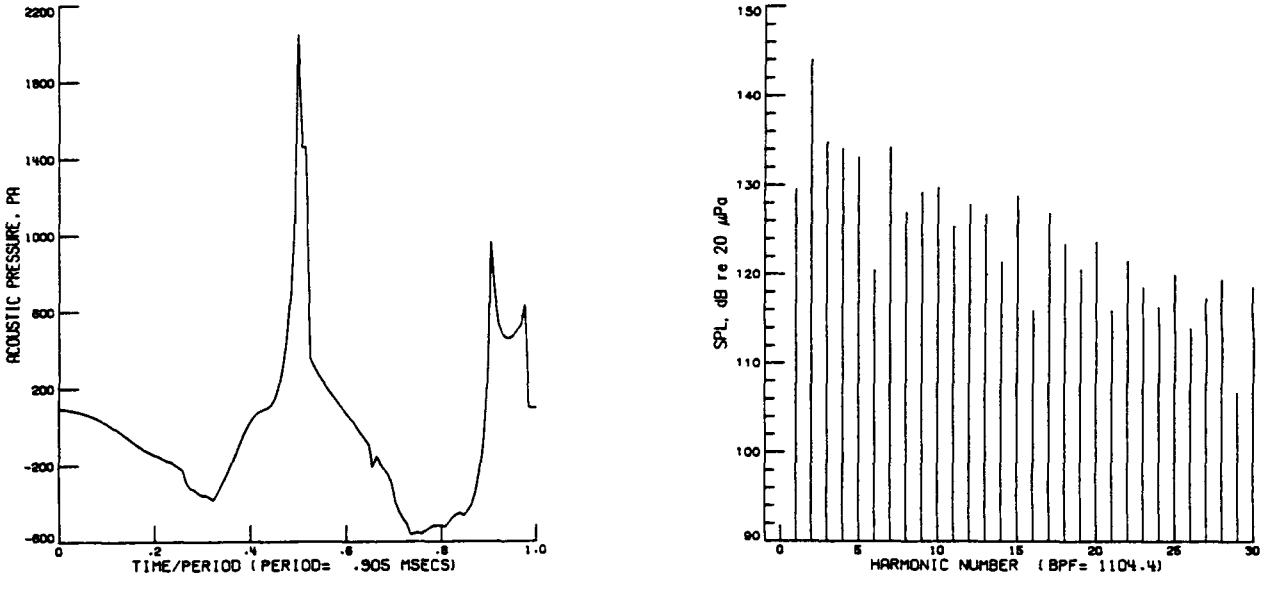

Figure 11: Total Noise for Example 2 - Model Counter Rotation Propeller System

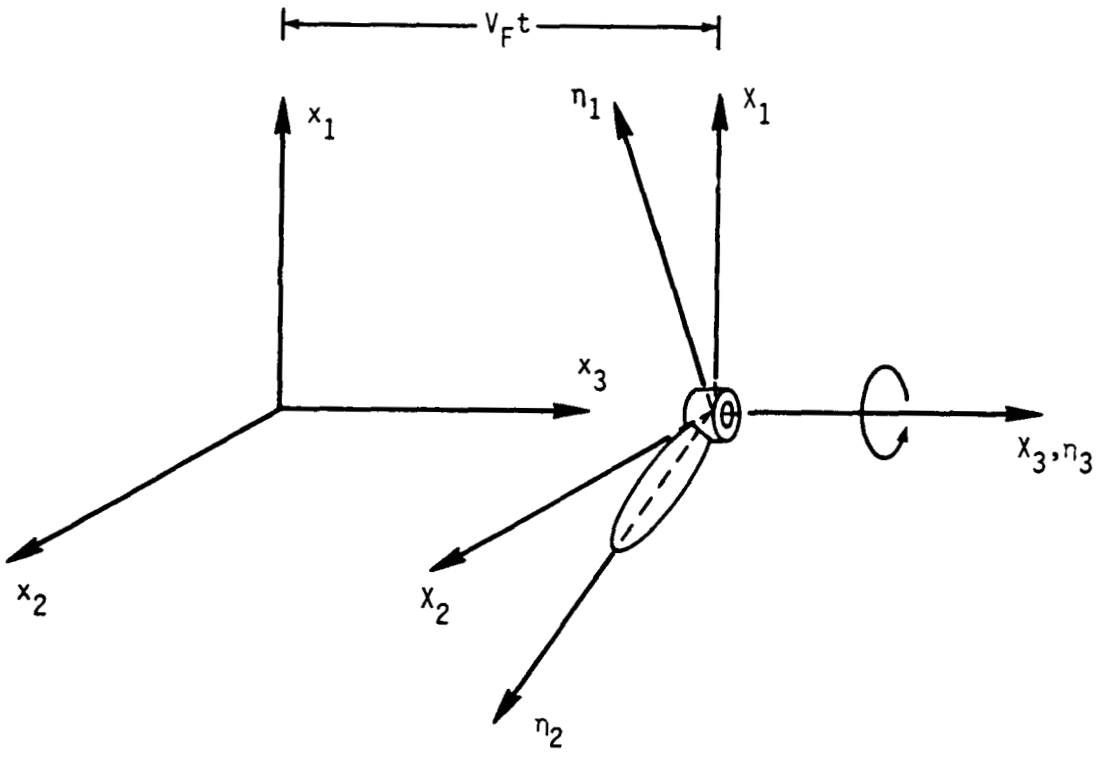

Figure 12: Coordinate Reference Frames [13]

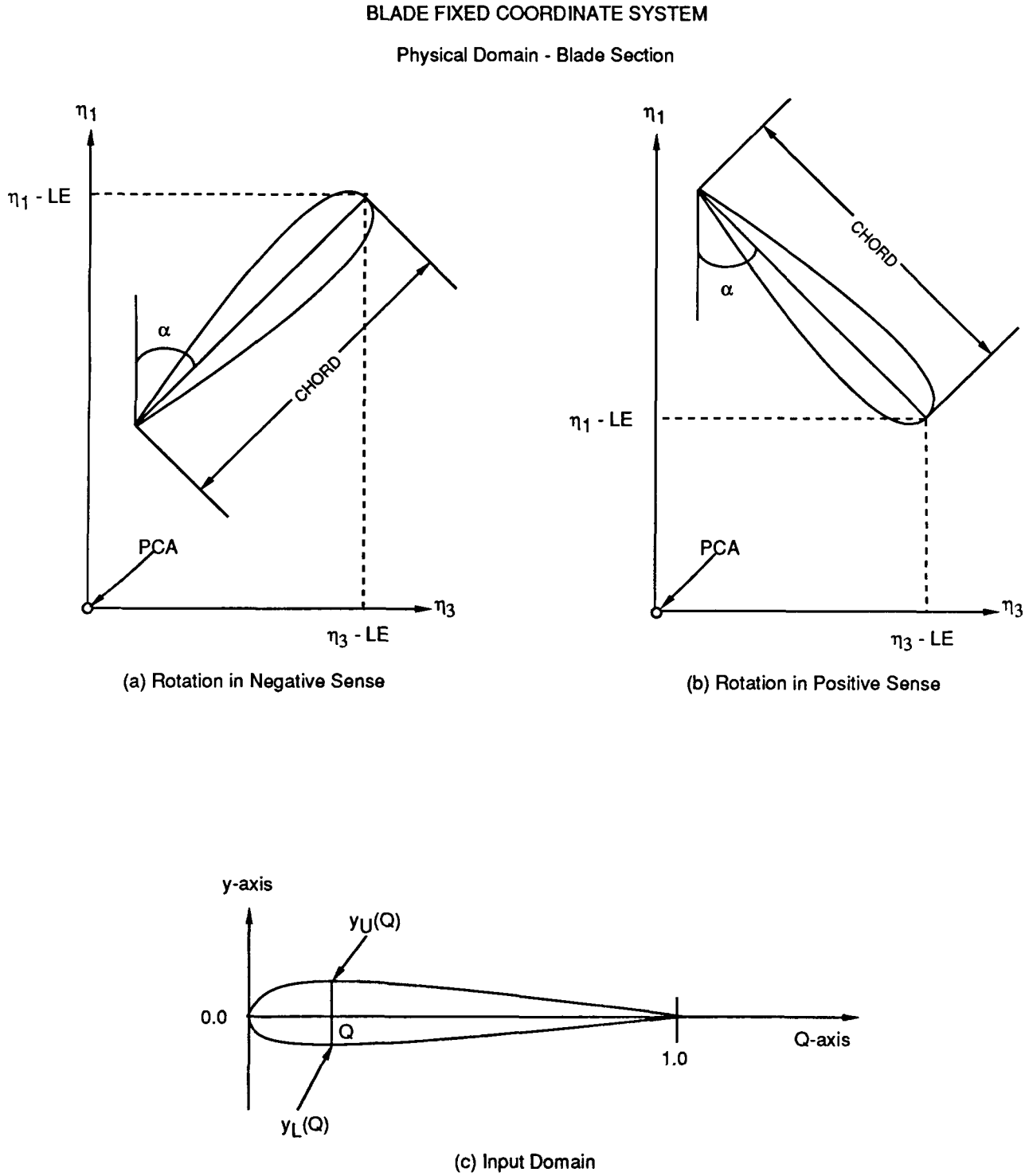

Figure 13: Blade Input Geometry

NASA
National Aeronautics and Space Administration

Report Documentation Page

1. Report No.	2. Government Accession No.	3. Recipient's Catalog No.
NASA CR-4208		

4. Title and Subtitle	5. Report Date
Users' Manual for the Langley High Speed Propeller Noise Prediction Program (DFP-ATP)	January 1989
	6. Performing Organization Code

7. Author(s)	8. Performing Organization Report No.
M. H. Dunn and G. M. Tarkenton	
	10. Work Unit No. 535-03-11

9. Performing Organization Name and Address	11. Contract or Grant No.
Planning Research Corporation Hampton, VA 23666	NAS1-18000
	13. Type of Report and Period Covered
12. Sponsoring Agency Name and Address	Contractor Report
National Aeronautics and Space Administration Langley Research Center Hampton, VA 2366505225	14. Sponsoring Agency Code

15. Supplementary Notes

Langley Technical Monitor: F. Farassat

16. Abstract

This manual describes the use of the Dunn-Farassat-Padula Advanced Technology Propeller (DFP-ATP) noise prediction program which computes the periodic acoustic pressure signature and spectrum generated by propellers moving with supersonic helical tip speeds. The program, developed at NASA Langley Research Center, has the capability of predicting noise produced by a single-rotation propeller (SRP) or a counter-rotation propeller (CRP) system with steady or unsteady blade loading. The computational method is based on two theoretical formulations developed by Farassat. One formulation is appropriate for subsonic sources, and the other for transonic or supersonic sources. Detailed descriptions of user input, program output, and two test cases are presented, as well as brief discussions of the theoretical formulations and computational algorithms employed.

17. Key Words (Suggested by Author(s))	18. Distribution Statement
Noise Prediction, Advanced Technology Propellers, Acoustics, Counter-Rotating Propellers.	Unclassified - Unlimited Subject Category 71

19. Security Classif. (of this report)	20. Security Classif. (of this page)	21. No. of pages	22. Price
Unclassified	Unclassified	48	A03

NASA-Langley, 1989